CONF-960543--33

UCRL-JC-124232
PREPRINT

Nuclear Diagnostics in Support of ICF Experiments

M. J. Moran
J. Hall

This paper was prepared for submittal to the
11th Topical Conference on High-Temperature Plasma Diagnostics
Monterey, CA
May 12-16, 1996

June 5, 1996

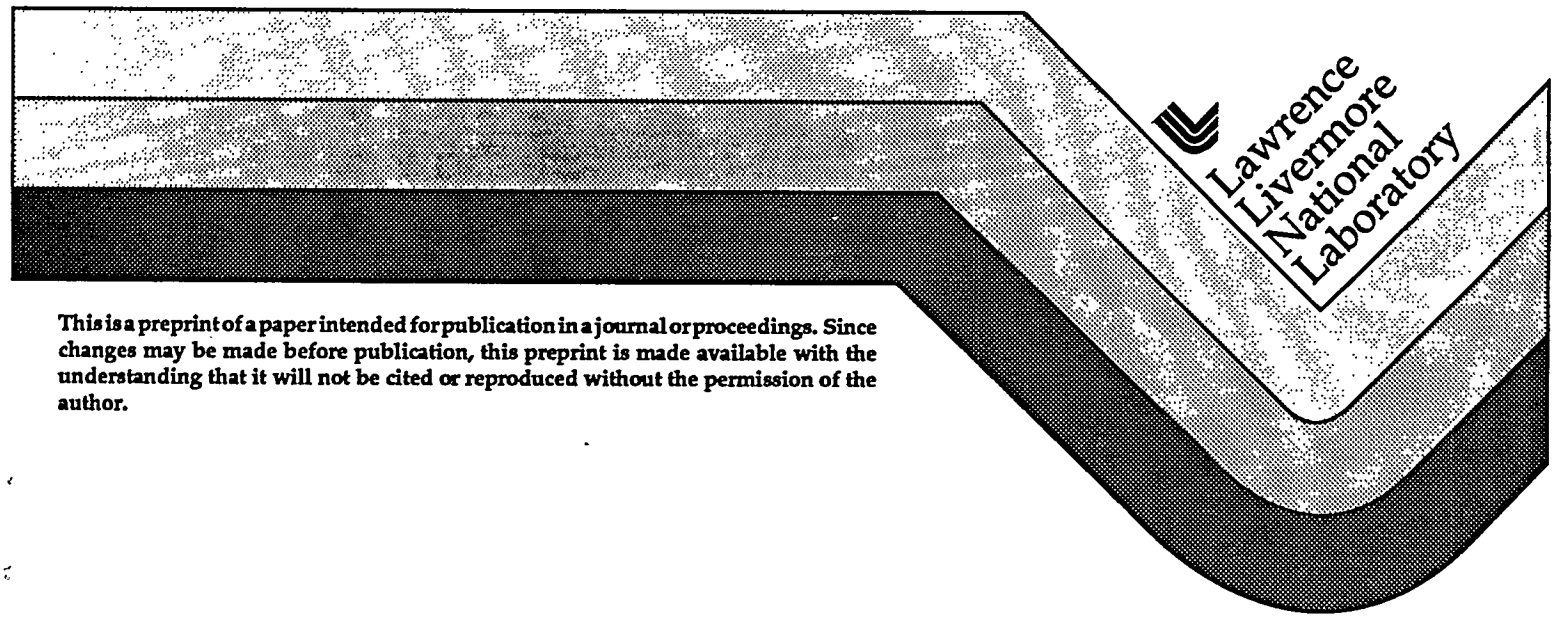

RB

Nuclear Diagnostics in Support of ICF Experiments

M. J. Moran and J. Hall

Lawrence Livermore National Laboratory

P.O. Box 808, Livermore, CA 94550

ABSTRACT

As the yields of Inertial Confinement Fusion (ICF) experiments increase to NIF levels new diagnostic techniques for studying details of fusion burn behavior will become feasible. The new techniques will provide improved measurements of fusion burn temperature and history. Improved temperature measurements might be achieved with magnetic spectroscopy of fusion neutrons. High-bandwidth fusion reaction history will be measured with fusion-specific γ-ray diagnostics. Additional energy-resolved γ-ray diagnostics might be able to study a selection of specific behaviors during fusion burn. Present ICF yields greater that 10^{13} neutrons are sufficient to demonstrate the basic methods that underlie the new techniques. As ICF yields increase, the diagnostics designs adjusted accordingly in order to provide clear and specific data on fusion burn performance.

I. Introduction

The approaching transition from low-yield to high-yield ICF experiments will be assisted by a suite of new diagnostic techniques that record the performance and study the behavior of laser-driven fusion-energy sources. The coming generations of ICF experiments will see increases in fusion yield by up to six orders of magnitude. The diagnostics will include measurements that have been used with low-yield experiments as well as new, less sensitive, techniques that record a broad range of data on fusion performance. The increasing fusion yields will lead naturally to increasing emphasis on new diagnostics for measuring a range of parameters that are related directly to fusion processes and performance. For example, it is likely that high-bandwidth γ-ray detectors will record fusion reaction histories and that proton-recoil detectors will measure yield and fusion neutron spectra. Together, the diagnostics will provide an overlapping and complementary collection of data that will be indispensable to understanding the performance of high-yield fusion sources. Before discussing details of some of these new diagnostics it is useful to review the nature of ICF sources and to show how their characteristics lead naturally to the kinds of diagnostics that can be used to study them.

II. ICF Source Characteristics

The emission of radiation from an ICF experiment takes place from a volume with a diameter less than 1 mm and with a duration of the order of 1 nanosecond. The spectrum of photon emissions span the entire range from infrared ($E_\gamma << 1$ eV) to γ-ray energies ($E_\gamma > 1$ MeV). Depending on the type of nuclear fuel, characteristic spectra of energetic neutrons also will be emitted.

Finally, as emission intensities increase, the sources also will produce significant charged particle fluxes.

Each of these different emissions, indicated schematically in Fig. 1, can serve as the basis of diagnostics that study different aspects of the fusion source. Infrared and optical measurements provide information on the timing and quality of the laser drive in the experiment. X-ray diagnostics have been used widely to study coupling of laser energy to the target, target motion and heating, and a wide range of parameters related to the evolution of laser-driven fusion events. Fusion performance itself has been studied mostly with a variety of sensitive neutron-based diagnostics: Neutron imaging has recorded the size and shape of the fusion source,[1] neutron activation has measured fusion yield,[2] and temporal measurements of neutron emission have studied both the history of the fusion reactions[3] and time-of-flight spectra for inferring source temperatures.[4]

As fusion yields increase less sensitive and perhaps more subtle measurements of neutron, γ-ray, and charged-particle emissions will probe additional details on the behavior of ICF sources. The possibilities for new diagnostics derive directly from the kinds of reactions that occur in a fusion source. Energy-resolved measurements of γ-ray emissions can serve as the basis of high-bandwidth measurements of fusion reaction history. The 16.7-MeV γ ray associated with (D,T) fusion is an excellent candidate for such a measurement:

$$(D,T) \rightarrow He^5 + \gamma(16.7\ MeV) \qquad (1)$$

Measurements of the fusion γ rays can provide a direct indication of the fusion reaction rate, and the results will free of temporal dispersion. However, the low relative intensity of this emission (branching ratio $\approx 5 \times 10^{-5}$) means that such measurements require ICF yields greater than 10^{13} neutrons. Furthermore,

since reactions such as (n,n'γ) also will produce measurable fluxes, γ-ray spectral measurements will be required in order to demonstrate that the anticipated measurements are "clean" and not distorted by emissions from other processes. These measurements also offer for the first time the possibility of performing a good measurement of the (D,T) fusion-γ spectrum. Due to high neutron backgrounds, previous laboratory measurements have had large uncertainties and have produced somewhat inconsistent results.[5]

The more familiar (D,T) reaction

$$(D,T) \rightarrow n(14.1\ MeV) + \alpha\ (2.5\ MeV) \qquad (2)$$

produces both neutrons and α-particles that can serve as the basis of unique diagnostics. Neutron-based diagnostics already have been refined as standard diagnostics for low-yield sources.[1-4] With higher-yield sources, accurate measurements of neutron spectra will provide clear indications of source temperature and deviations from Maxwellian distributions.[6] Such data is fundamental to understanding the physical conditions in a fusion source. Spectral and spatial measurements of the α-particle distributions provide different kinds of information. Because of the rapid energy loss of slow charged particles, α-particle spectra can indicate the "ρr" density characteristic, and angular distributions can suggest symmetries or asymmetries in the sources.[7]

As fusion yields increase so-called "secondary" and "tertiary" reactions can provide more subtle information on fusion processes. The reaction

$$n(14\ MeV) + n(14\ MeV) \rightarrow n'(> 14\ MeV) + n''(< 14\ MeV) \qquad (3)$$

between 14 MeV neutrons is depends on the neutron intensity of the source. High-energy neutron fluxes produced by this reaction become measurable only for very intense fusion sources. Multiple collisions that produce neutrons

with energies above 28 MeV become relatively weak, but very sensitive, indicators of source intensity. For charged particle, the reaction

$$D^* + He^3 \rightarrow p + \alpha \qquad (4)$$

between "thermal" deuterons and He^3 (often "seeded" into the target). This reaction is interesting because the proton spectrum is a sensitive indicator of the initial deuteron "thermal" distribution.[7]

III. Basic Diagnostic Interactions

Nuclear diagnostics derive from specific interactions with energetic radiation emitted by the source. "Direct" interactions which indicate the presence of a particular radiation have been the basis of nuclear diagnostics for low-yield ICF experiments. For example, neutron imaging of a fusion source has employed scintillators and imaging systems that measure neutron fluences, generally without spectral or temporal information.[1] Similarly, the Large Neutron Scintillator Array (LaNSA) uses scintillation-detector arrays to measure neutron time-of-flight spectra.[4]

"Indirect" interactions can be used to design diagnostics with higher-yield sources to recover a broader range of data than is possible with "direct" interactions. Indirect interactions work by converting incident radiation to forms which can be detected with high efficiency and good definition, as shown schematically in Fig. 2. Indirect interactions tend to be inefficient, but many are extremely well defined and can provide detailed information about the source radiation of interest. Important examples of indirect interactions include neutron-to-proton "conversion" with (n,p) ("proton recoil") scattering and γ-to electron conversion with Compton scattering or pair production. Each of these interactions has an accurately known cross section, and they can serve as bases of accurate spectral measurements of neutrons and γs. These reactions

are especially useful for diagnostics because they produce charged particles that can be detected with high efficiency, high bandwidth, and can be spectrally resolved with magnetic analyzers.

Neutron-to-proton conversion

With proton scattering, an elastic collision between an incident neutron with kinetic energy En and a target proton, typically in a thin hydrogenous foil (of polyethylene, e.g.), produces a recoil proton with kinetic energy E_p given by

$$E_p = E_n \cos^2\theta, \tag{5}$$

where θ is the angle between the initial neutron trajectory and that of the scattered proton (see Fig. 2). The cross section for this interaction is known with a accuracy of a few percent, is isotropic in the center-of-mass frame, and can be written in the laboratory frame as[8]

$$\frac{d\sigma_{n,p}}{d\Omega} = 223 \cos\theta \text{ mb/steradian.} \tag{6}$$

This might be considered a relatively large cross section, but experimental realities dictate that the overall efficiency of the conversion generally is quite small. Geometrically, incident solid angle fractions typically are much less than 10-3, with comparable detection solid angles. In order to minimize energy loss and angular spreading (due to Molière scattering[8]), scattering foils generally have thicknesses less than 4×10^{21} p/cm^2 ($\approx$ .05 cm CH_2), with a corresponding conversion efficiencies less than 2×10^{-4} p/n-ster. This suggests that present (D,T) yields of about 10^{13} are barely adequate ($\approx$ 1000 recoil protons) to produce measurable signals in a realistic experimental arrangement.

γ-to electron conversion

The two main mechanisms for (γ,e) conversion have significant differences that allow considerable flexibility in diagnostic design. Pair

production and Compton scattering both have cross sections that can be computed accurately, and they both produce beams of relativistic electrons that can be detected by a number of techniques. The scattered electron beams have peak energies that are comparable to the incident γ-ray energy and are collimated to within an angle given roughly by $\Delta\theta \approx 1/(2E_\gamma)$. Beyond this, however, the two mechanisms are quite different.

Pair production is the complete conversion of the γ ray energy into an electron-positron pair.[9] However, since this is a three-body interaction (it occurs in the vicinity of an atomic nucleus that absorbs some of the recoil momentum), there is no unique energy-angle relationship for the recoil particles. This means that if pair production is to be used for γ-ray spectroscopy, then spectroscopy must be performed on the correlated pairs of particles - generally a difficult task. Also, pair production has an incident γ ray energy threshold of 1.02 MeV, in order to be able to produce the particle pair. The total pair-production cross section is roughly proportional to E_γ^2 and to Z^2, where Z is the atomic number of the converter material. Overall, pair production often has a larger total cross section than Compton scattering, and the energy threshold can provide useful discrimination against lower-energy γs. In a thick high-Z target, (γ,e) conversion efficiency can approach 10%, although the transmitted beam will be highly dispersed in energy and angle.

Compton scattering is basically elastic collisions that produce recoil electrons (and photons) from a target foil.[10] Here, the cross section is specified by the Klein-Nishina formula. Since this cross section features a specific energy-angle relation for the recoil electrons, measurements of Compton electron energy spectra can be used to measure incident γ-ray spectra. Again, the recoil electrons are confined to a beam with angular collimation given roughly by $1/(2E_\gamma)$. The peak energy (in the forward direction) is only

slightly less than Eγ. Compton scattering is only weakly dependent on photon energy and is proportional to the electron density of the target material. Although the total cross section is less than for pair production, is possible to choose converter targets that have a forward differential cross section that is greater than for pair production. Thus, the design of the (γ,e^-) converter for a diagnostic presents options that must be evaluated in terms of the requirements and capabilities of the particular technique being used.

γ-ray spectroscopy

There are many different interactions in a fusion source that can produce signals in γ-ray detectors. Uncertainties in the nature of γ-ray signals can be removed with spectral measurements that demonstrate that specific reactions are associated with the recorded signals. Here, even modest energy resolution will be useful in identifying the sources of recorded signals. For example, if the spectrum has a relatively uniform low level, except for a prominent peak at around 16.7 MeV, then it is clear that fusion γ rays dominate the spectrum and any associated data. Measurement of the spectrum is problematic, however, because the spectrum is relatively weak and it is emitted in a single flash. Several different techniques are being evaluated for possible measurement of ICF γ-ray spectra.

The cloud chamber technique, indicated schematically in Fig. 3, infers a spectrum by measuring the radii of curvature of recoil electrons under the influence of a magnetic field in a fluid that produces a temporary visible "track" along the particle trajectory. This technique has been used extensively in high-energy physics for particle diagnostics. Application to measuring ICF γ-ray spectra is possible, but significant research and engineering effort probably will be required. A group a Sandia National Laboratories is pursuing this approach.[11]

Compton magnetic spectrometers are another possible approach.[12] Here, as indicated in Fig. 4, Compton electrons from a low-Z converter are dispersed in energy by a magnetic analyzer that focuses different energies at different points along a specified line at the spectrometer output. Detector arrays or position-sensitive detectors can measure the spectral distribution of electrons, which in turn can be used to infer the corresponding γ-ray spectrum. There are numerous designs that have been developed for this type of measurement and they match well with single-pulse experiments, but they tend to be rather insensitive, due to collection fraction and conversion efficiency.

Another example might be called scintillator calorimetry.[13] Here, the energy of a photon and all of its recoils is converted light in a scintillating crystal (see Fig. 5). The height of the optical pulse produced by a photomultiplier coupled to the scintillator is related to the energy of the initial photon and its energetic recoils. Over time, pulse-height analysis of signals from such a detector can produce a distribution that indicates the spectrum of incident γ-rays.[13] Alternatively, a large spatial array of detectors that respond to individual γ rays from a single intense pulse can generate a collections of pulses whose pulse-height distribution indicates the spectrum of the pulsed source. This approach is sensitive and well understood, but it may will be expensive to construct (many crystals and detectors) and will produce data having poorly defined pulsed-height distributions (due to small crystals).

IV. Examples of New Diagnostics

γ-ray Cherenkov detector

High-bandwidth recording of fusion γ-ray production will provide reliable high-quality data on the fusion performance of high-yield ICF targets. Two recent experiments have recorded the prompt γ-ray emission from ICF sources

with yields in excess of 10^{13} (D,T) neutrons. One approach is to use a high-bandwidth photoconductive detector.[14] The other approach uses a high-bandwidth Cherenkov detector to measure the γ-ray emission rate. Figure 6 shows a schematic diagram of the detector design. γ rays from the source pass through a thick Pb collimator and strike a (γ,e^-) converter. When the converter is Be, Compton scattering dominates the conversion process; and when the converter is Pb, pair production dominates. The conversion efficiency is about than 1%. Electrons (and positrons) are scattered in the forward direction where they enter a transparent plastic cone that serves as a Cherenkov radiator.

The relativistic electrons generate Cherenkov light as they travel through the plastic because their speed, $v \approx c$ (the speed of light in a vacuum), is greater than the speed of light in that medium, c/n, where $n \approx 1.5$ is the refractive index of the plastic. Cherenkov light under these conditions is an electromagnetic shock wave, with a broadband spectrum that extends from the far infrared into the ultraviolet regions, is emitted into a symmetric conical distribution with a half angle of 48°.[15] Since Cherenkov light is coherent with respect to the motion of the electron (it can display interference fringes), it has effectively an instantaneous response and can be used for high-bandwidth detection of the γ rays. The truncated conical geometry of the radiator provides total internal reflection for the Cherenkov cone and reflects it into a roughly forward-directed beam of light. A toroidal lens that was machined into the base of the cone serves to collimate the light further as it leaves the cone. An off-axis parabola turns the beam and focuses it at an off-axis point. An additional turning mirror reflects the focusing beam into a forward-facing microchannel-plate photomultiplier (PM). This folded geometry enables the detector to be placed in confined areas external vacuum chamber, but close to the ICF source.

Figure 7 shows signals generated by the Cherenkov detector on three different ICF events. With 1-cm Be and 3-mm Pb converters, small signals were recorded at the expected γ-ray emission time (≈ 3 ns). The signals are ≈ 0.7-ns 150-mV "blips" on the leading edge of large (> 30 volts) neutron-pulse signals. A "background" test with black tape over the PM produced a much reduced signal. Here, the detector was located about 60 cm from the source, and the fusion yield was about $2x10^{13}$ (D,T) neutrons. These signals probably are associated with fusion γ rays, but non-fusion γs also are present. Non-fusion γs are evident in the pulse near 4.5 ns with the Be converter. The γ rays evidently were produced by (n,n'γ) interactions in a tungsten converter that was located about 10 cm from the ICF target. Interestingly, these results appear to demonstrate also that the conversion threshold for pair production in Pb prevents these lower-energy γs from producing measurable signals with the Pb converter. Overall, this data demonstrates that ICF yields have reached levels where fusion γ-rays can be used for diagnostic measurements, but that higher yields will be needed to produce high-quality data.

A scintillation spectrometer

With prototype detectors beginning to record fusion-γ data, new approaches to measuring γ-ray spectra must be developed also. One approach that is being studied is to use an array of microcrystals and an intensified CCD camera to generate pulse-height distribution measurements of the γ-ray spectra. This approach is convenient and affordable, but it is not clear that adequate resolution can be achieved over the desired energy range of, roughly, 1 to 20 MeV. As a feasibility test of this approach, a micro-crystal array of BGO scintillators (0.6x0.6x40 mm) was optically coupled to an intensified CCD camera. A Co^{60} 1-MeV γ-ray source excited the scintillator array, and Fig. 8 shows the

corresponding image recorded by the CCD. Here, background image was subtracted from the data in order to remove thermally generated counts.

Figure 8 shows an image covered with dim and bright spots. The small bright spots represent direct single interactions in the CCD chip with the γ rays. The larger dimmer spots represent images of interactions in single scintillator "pixels" with single γ rays. The dim spots represent only about three counts above the background level, but they demonstrate that single interactions can be imaged in this type of system with γ-ray energies as low as 1 MeV. If this system were used to measure γ-ray spectra, then the energy resolution would vary as $1/\sqrt{N}$, where N is the number of counts (above background) in the image of the pixel. N should be roughly proportional to the energy of the initial γ ray, so that energy resolution improves as energy increases.

The test above does not show useful energy resolution, but it has demonstrated that the lower energy single interactions can be observed in an image. With improvements in optical collection, this system might achieve resolution in the range of 30 - 50 percent for 1-MeV photons, with significant improvement at higher energies. This result demonstrates that micro-scintillator detectors might be capable of measuring absolute γ-ray spectra from 1 to 20 MeV. The resolution will be modest, but it should be capable of evaluating characteristic features for their usefulness in ICF diagnostics. For example, showing that the 16.7-MeV fusion γs are dominant in that spectral region will lend credibility to their use for studying fusion reaction histories. Similarly, 4.4-MeV (n.n'γ) in carbon or 6.1-MeV (n.n'γ) in oxygen might be shown to be useful for studying the concentrations of those species in the fusion volume.

A proton-recoil neutron detector

Accurate convenient yield measurements and studies of fusion neutron spectra are two kinds of measurements that can be performed with proton-recoil detectors as ICF fusion yields increase. Of these two, yield measurements are the easiest to perform, and they are becoming feasible with present ICF yields. This techniques illustrated by the simple experimental arrangement shown in Fig. 9.

The (n,p) detection system works as follows. Neutrons from the source are collimated by a 2.5-cm diameter aperture at 100 cm from the source (solid angle fraction $\approx 3.9 \times 10^{-5}$) before they strike a polyethylene (CH_2) foil with a thickness of 0.05-cm ($\approx 4.3 \times 10^{21}$ H/cm^2). The detector is positioned to receive recoil protons at an angle of 30°, corresponding to an (n,p) scattering cross section of 0.193 barns/proton-steradian. A 1-cm diameter aperture 30 cm from the CH^2 foil (solid angle $\approx 8.7 \times 10^{-4}$ steradians) collimates the recoil protons. Before they strike the detector, an aluminum barrier (thickness $\approx$ 0.05 cm) ranges the recoil proton energy down to about 5 MeV. This reduced energy can be absorbed completely in the 500-μm thick depletion region of the 1-cm^2 silicon PIN diode. Since the proton energy is converter to electron-hole pairs in the depletion region (3.67 eV/pair), they are detected with high gain ($\approx 1.5 \times 10^6$).

Overall, this system combines to have a net sensitivity of 1.36×10^{-15} amp/(neut/sec). For a yield of 10^{13} (D,T) neutrons and a 50-ohm system, this corresponds to a 0.68-volt signal. This must be compared with the direct neutron background signal in the PIN diode. An estimated neutron energy deposition in the PIN diode of 8.5×10^{-8} erg-cm^2/(gm-neut) (from neutron cross-section tables) gives a sensitivity of about 2.7×10^{-16} amps/neut-sec. The 1-cm^2 detector 3 meters from the 10^{13} neutron source would have a direct signal of 0.44 amps, or 22 volts (generated by $\approx$ 300 recoil protons). Thus, we see that

even though the proton-recoil signal is measurable, it is much smaller than the background signal. This can be dealt with either by increasing the efficiency of the proton-recoil geometry (by increasing the neutron collimator and CH_2 area, for example), or by providing neutron shielding for the PIN diode. Experimentally, background signals can be measured directly with a second PIN diode mounted behind the proton detector. The background signals then can be subtracted accurately from the proton-recoil signal.

The discussion above shows that proton-recoil measurements of yield are becoming feasible. As ICF yields increase further, more sophisticated techniques can be used to measure the fusion neutron spectra with recoil protons. Such measurements will require yields in excess of 10^{15} neutrons. The spectra can be measured with magnetic spectrometers and linear arrays. This system would be much more compact and convenient to use than traditional time-of-flight measurements of the spectrum. The data also would be interesting in that it would represent a direct measurement of neutron energy spectrum and would be less vulnerable to distortions from scattered neutron backgrounds

V. Numerical modeling of experiments

A discussion of nuclear diagnostics on NIF experiments must include some description of Monte Carlo calculations that can be used to describe the radiation environment of the experiments, and details of diagnostic response functions. These calculations will become a routine and indispensable part of diagnostic design and interpretation on NIF experiments. There are several reasons for this trend. First, the scale of NIF experiments will become so large and expensive that computer calculations will be used to optimize diagnostic design and minimize data loss. The expense and repetition rate of NIF experiments will require that diagnostics be as thoroughly designed as possible when they

are installed. Second, the computer codes and computer resources have been advancing rapidly during the past ten years, and they are available now for relatively modest cost. Previously, adequate computational hardware and software required expensive development efforts, and their capabilities were far less than is available today.

Finally, these developments mean that extensive calculations can be performed both to characterize extensive details of the experimental environment, as well as details of diagnostic design and performance. For example, it has become a straightforward exercise to input the entire experimental vessel geometry (distances, sizes, materials, etc.) in order to model details of the radiation flux that is incident on any portion of a diagnostic. In many cases, it also has become possible to model details of the response of diagnostic components to details of the incident radiation, so that realistic comprehensive predictions of diagnostic performance can be calculated.

These new capabilities will be more than desirable conveniences. As fusion yields increase, new diagnostics will be designed that probe ever more intimate aspects of fusion behavior. The data from such diagnostics often will be very complex, and detailed understanding of diagnostic characteristics will be a prerequisite to interpreting the data with confidence. In this way, new sophisticated diagnostics and detailed computer modeling will combine to provide detailed and compelling interpretations of the data.

VI. Conclusion

The steady increases that are expected in the yields of future ICF experiments will make possible a variety of new diagnostics that study the fusion processes directly. The diagnostics will be based on characteristic γ-ray , neutron, and charged-particle radiations associated with fusion processes. The

new diagnostics will be designed to measure specific characteristics of these radiations, such as absolute intensity, spectra, and spatial distributions. These data will reflect the processes taking place within the fusion source and will help us understand how to optimize the performance of ICF systems. This work was performed under the auspices of the U.S. Department of Energy by the Lawrence Livermore National Laboratory under Contract number W-7405-ENG-48.

References:

1 D. Ress, R.A. Lerche, R.J. Ellis, and S.M. Lane, *Rev. Sci. Instrum.* 59, 1694 (1988).

2 Nelson, puck yield

3 R.A. Lerche, D.W. Phillion, and G.L. Tietbohl, *Rev. Sci. Instrum.* 66, 933 (1995).

4 M.B. Nelson and M.D. Cable, *Rev. Sci. Instrum.* 63, 4874 (1992).

5 J.E. Kammeraad, J. Hall, K.E. Sale, C.A. Barnes, S.E. Kellogg, and T.R. Wang, Phys. Rev. C 47, 29, (1993).

6 H. Brysk, *Plasma Physics* 15, 611 (1973).

7 R. Petrasso, C.K. Li, M.D. Cable, S.M. Pollaine, W.S. Haan, T.P. Bernat, J.D. Kilkenny, S. Cremer, J.P. Knauer, C.P. Verdon, and R.L. Kremens, Paper C3 (these proceedings), preprint PFC/JA-95-40, Plasma Fusion Center, M.I.T. (1996).

8 E. Segrè, ed., *Experimental Nuclear Physics*, Vol. 1, John Wiley and Sons, New York (1953).

9 R.D. Evans, *The Atomic Nucleus*, McGraw-Hill, Ney York, (1955).

10 A.T. Nelms, *National bureau of standards circular 542*, U. S. Government Printing Office, (1953).

11 R. Leeper, Personal communication.

12 E. Segrè, ed., *Experimental Nuclear Physics*, Vol. 3, John Wiley and Sons, New York (1959).

13 G.F. Knoll, *Radiation Detection and Measureent*, John Wiley and Sons, New York (1979).

14 S.E. Caldwell, T.L. Petersen, and C.S. Young, Paper P3.24, (these proceedings).

15 J.V. Jelley, *Cerenkov Radiation and Its Applications*, Permagon, New York (1958).

Figure Captions

Figure 1 Generic fusion source: radiation emissions.

Figure 2 Geometry for indirect interactions.

Figure 3 Schematic diagram of cloud chamber spectrometer.

Figure 4 Schematic diagram of Compton spectrometer

Figure 5 Schematic diagram of scintillator spectrometer.

Figure 6 Prototype Cherenkov detector.

Figure 7 Signals from prototype Cherenkov detector.

Figure 8 Scintillator image with γ-ray illumination.

Figure 9 Simple proton-recoil detector geometry.

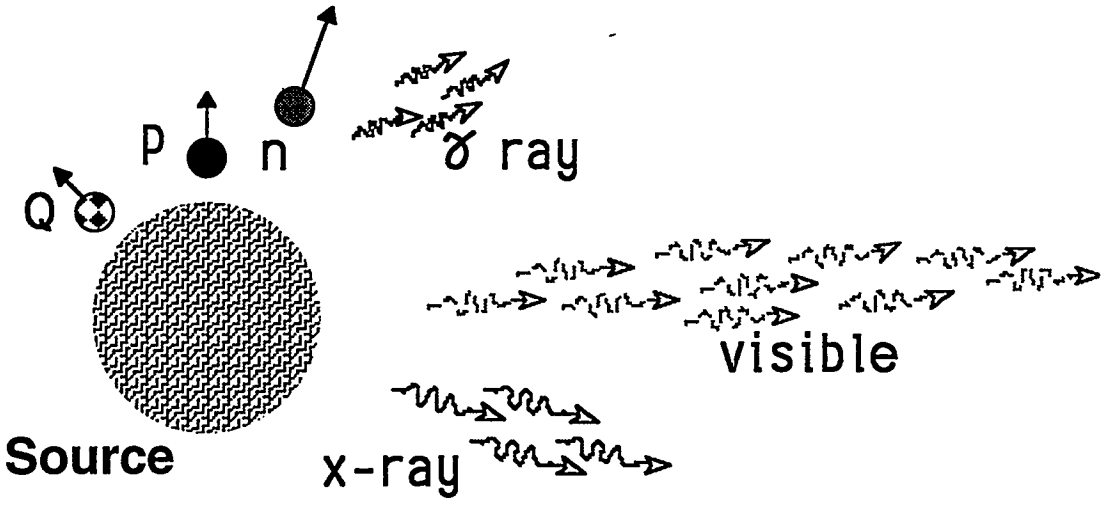

Figure 1 Generic fusion source: radiation emissions.

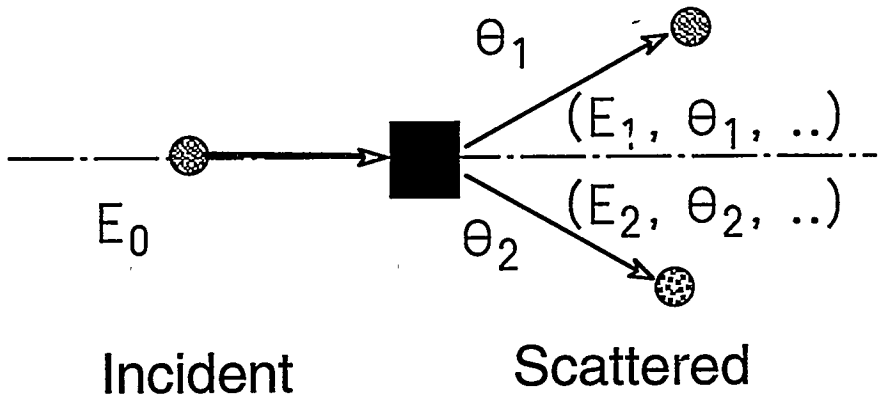

Figure 2 Geometry for indirect interactions.

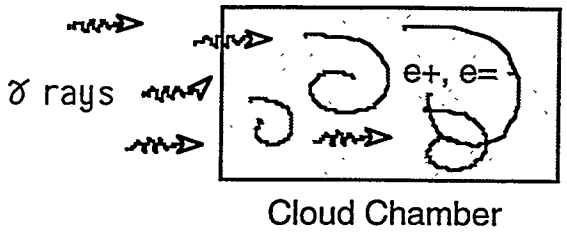

Figure 3 Schematic diagram of cloud chamber spectrometer.

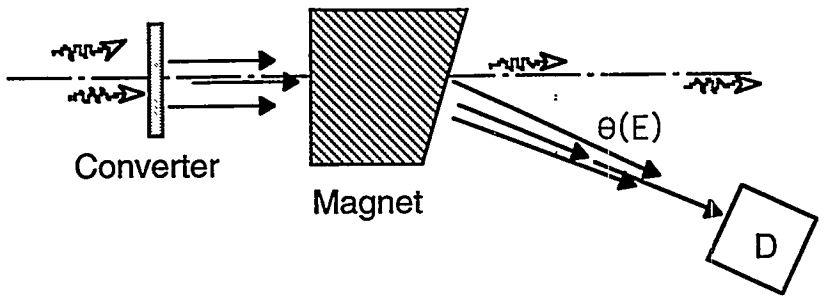

Figure 4 Schematic diagram of Compton spectrometer

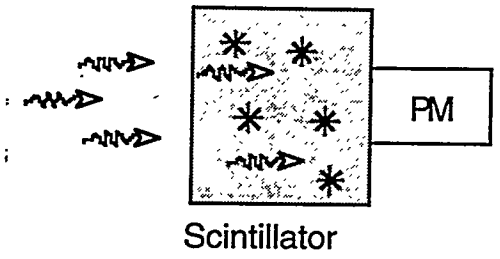

Figure 5 Schematic diagram of scintillator spectrometer.

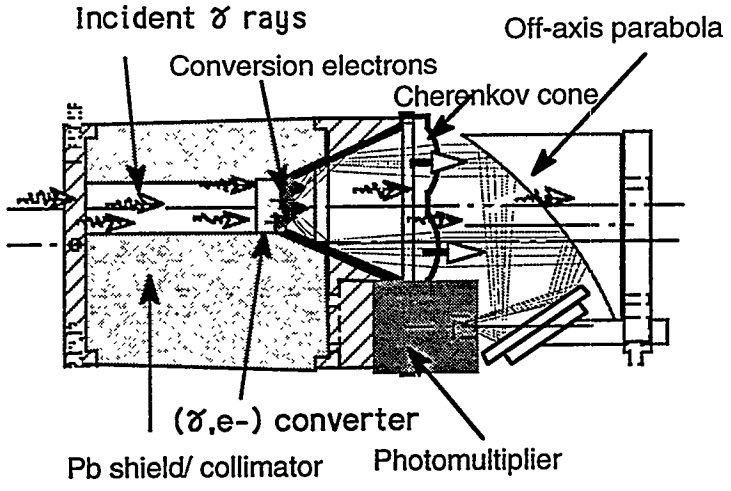

Figure 6 Prototype Cherenkov detector.

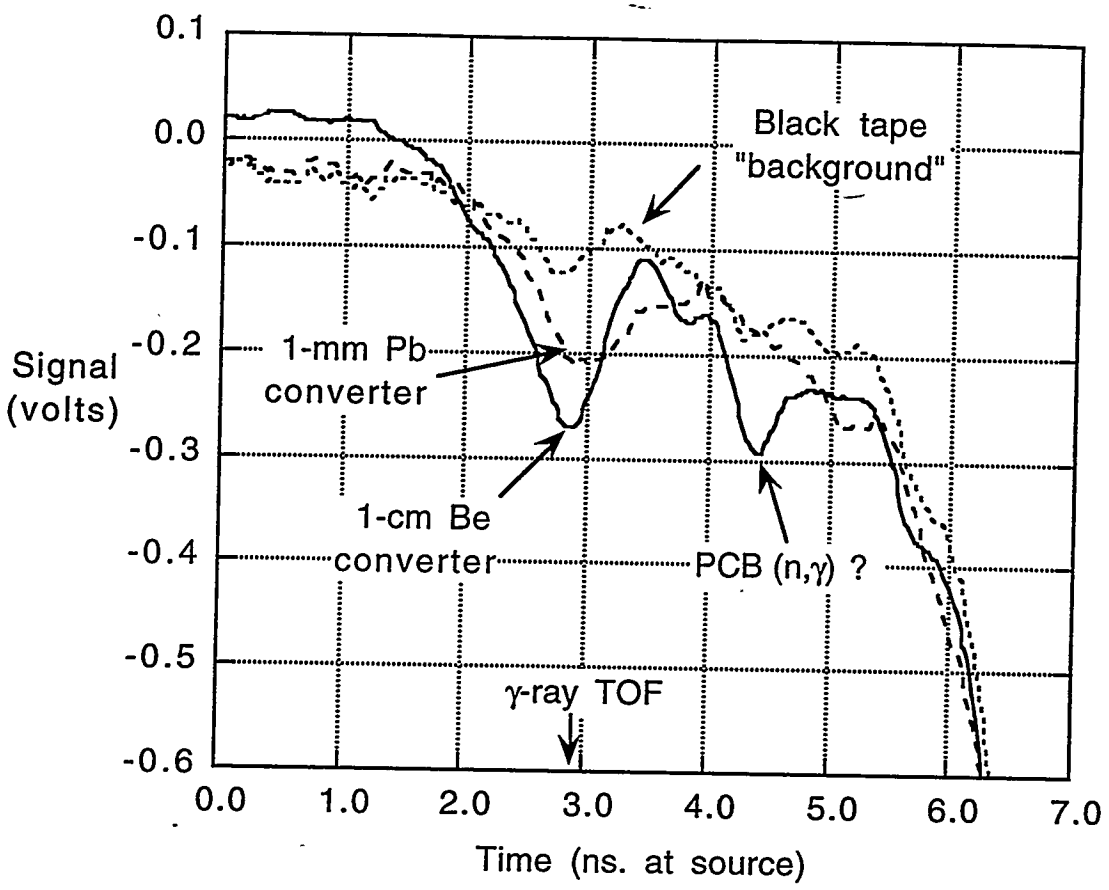

Figure 7 Signals from prototype Cherenkov detector.

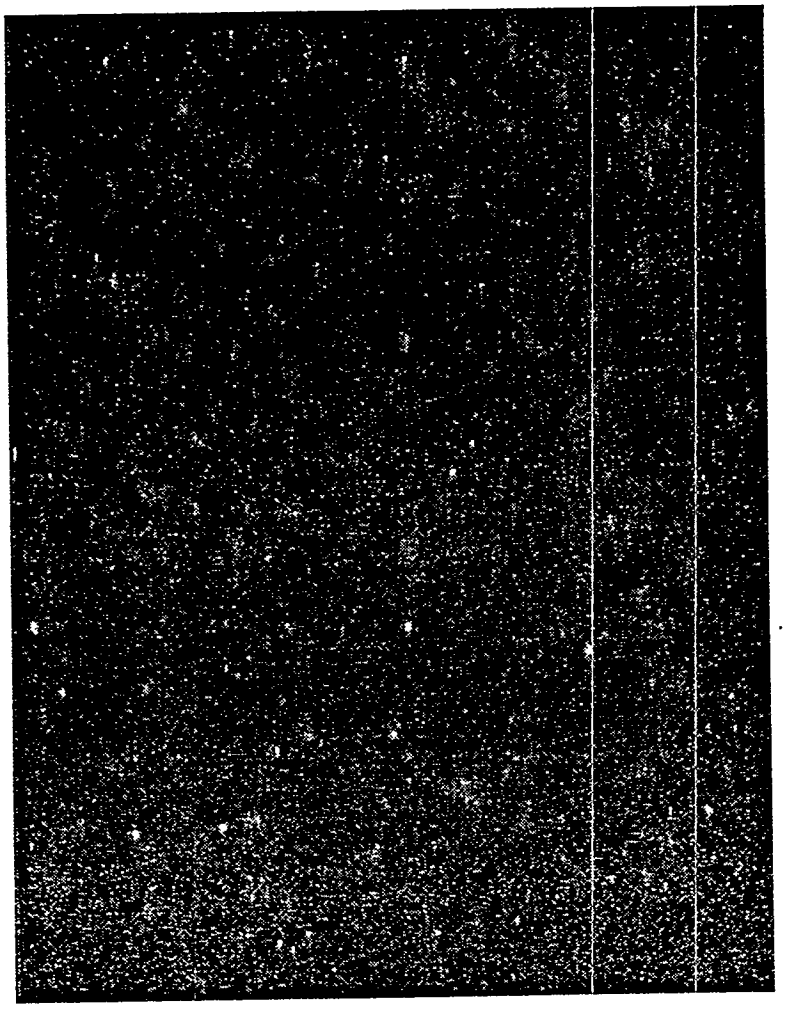

Figure 8 Scintillator image with γ-ray illumination.

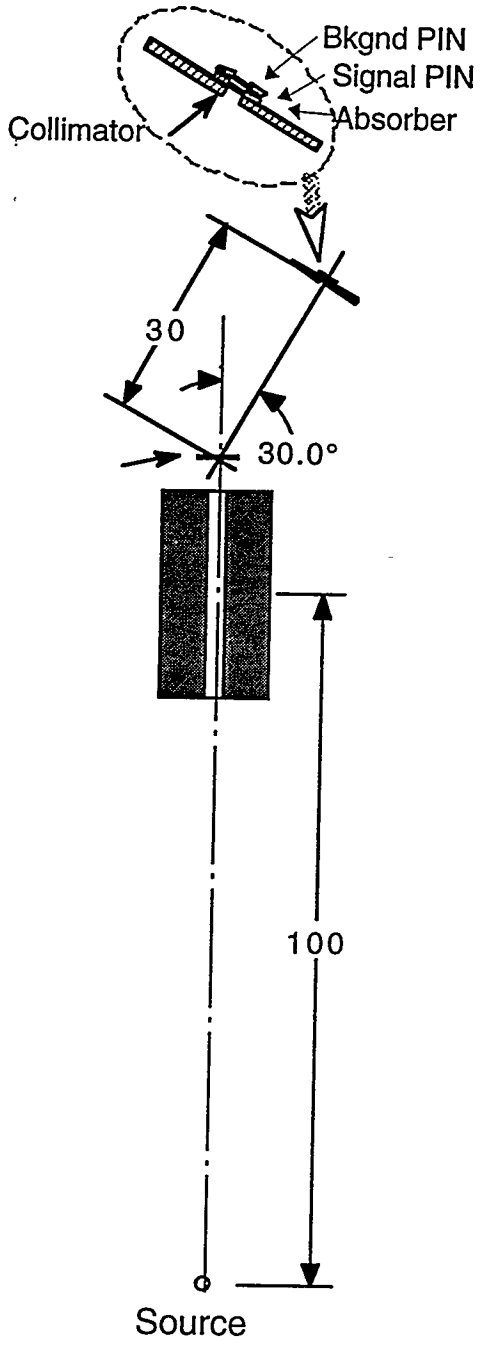

Figure 9 Simple proton-recoil detector geometry.